High-Temperature Shock Tube Measurements of Methyl Radical Decomposition†

Venkatesh Vasudevan,* Ronald K. Hanson, David M. Golden, Craig T. Bowman, and David F. Davidson

High Temperature Gasdynamics Laboratory, Mechanical Engineering Department, Stanford University, Stanford, California 94305

Received: November 21, 2006; In Final Form: December 22, 2006

We have studied the two-channel thermal decomposition of methyl radicals in argon, involving the reactions $CH_3 + Ar \rightarrow CH + H_2 + Ar$ (1a) and $CH_3 + Ar \rightarrow CH_2 + H + Ar$ (1b), in shock tube experiments over the 2253−3527 K temperature range, at pressures between 0.7 and 4.2 atm. CH was monitored by continuous-wave, narrow-line-width laser absorption at 431.1311 nm. The collision-broadening coefficient for CH in argon, $2\gamma_{CH-Ar}$, was measured via repeated single-frequency experiments in the ethane pyrolysis system behind reflected shock waves. The measured $2\gamma_{CH-Ar}$ value and updated spectroscopic and molecular parameters were used to calculate the CH absorption coefficient at 431.1311 nm (23194.80 cm^{-1}), which was then used to convert raw traces of fractional transmission to quantitative CH concentration time histories in the methyl decomposition experiments. The rate coefficient of reaction 1a was measured by monitoring CH radicals generated upon shock-heating highly dilute mixtures of ethane, C_2H_6, or methyl iodide, CH_3I, in an argon bath. A detailed chemical kinetic mechanism was used to model the measured CH time histories. Within experimental uncertainty and scatter, no pressure dependence could be discerned in the rate coefficient of reaction 1a in the 0.7−4.2 atm pressure range. A least-squares, two-parameter fit of the current measurements, applicable between 2706 and 3527 K, gives k_{1a} ($cm^3\ mol^{-1}\ s^{-1}$) = $3.09 \times 10^{15} \exp[-40700/T\ (K)]$. The rate coefficient of reaction 1b was determined by shock-heating dilute mixtures of C_2H_6 or CH_3I and excess O_2 in argon. During the course of reaction, OH radicals were monitored using the well-characterized $R_1(5)$ line of the OH A−X (0,0) band at 306.6871 nm (32606.52 cm^{-1}). H atoms generated via reaction 1b rapidly react with O_2, which is present in excess, forming OH. The OH traces are primarily sensitive to reaction 1b, reaction 9 ($H + O_2 \rightarrow OH + O$) and reaction 10 ($CH_3 + O_2 \rightarrow$ products), where the rate coefficients of reactions 9 and 10 are relatively well-established. No pressure dependence could be discerned for reaction 1b between 1.1 and 3.9 atm. A two-parameter, least-squares fit of the current data, valid over the 2253−2975 K temperature range, yields the rate expression k_{1b} ($cm^3\ mol^{-1}\ s^{-1}$) = $2.24 \times 10^{15} \exp[-41600/T\ (K)]$. Theoretical calculations carried out using a master equation/RRKM analysis fit the measurements reasonably well.

Introduction

The thermal decomposition of methyl radicals proceeds via two competing reaction pathways

$$CH_3 + Ar \rightarrow CH + H_2 + Ar \qquad (1a)$$

$$CH_3 + Ar \rightarrow CH_2 + H + Ar \qquad (1b)$$

Reactions 1a and 1b play an important role in the high-temperature combustion and pyrolysis of hydrocarbon fuels such as natural gas. For example, rate coefficients of both methyl decomposition pathways need to be well-established to correctly capture the CH peak height in elevated-temperature methane oxidation experiments. This is evident from the sensitivity plot shown in Figure 1a.

The rate coefficient of reaction 1a has been measured by Hanson and co-workers[2,3] and Markus et al.[4] Dean and Hanson[2] and Markus et al.[4] monitored CH by ring dye laser absorption near 431.1 nm and determined k_{1a} from the measured CH profiles. Over nearly the same temperature range, significantly different rate coefficients (by a factor of ∼5) were reported in the two studies. This was subsequently attributed by Markus et al.[5,6] to a large, unexplained pressure dependence for CH formation between 0.3 and 3.5 bar. Values for k_{1a} have also been obtained in a shock tube study of the $CH + O_2$ reaction system[3] by fitting measured CH concentration time histories using a detailed chemical kinetic mechanism. The inferred rate coefficient data were found to be consistent with the measurements of Dean and Hanson[2] at ∼1 bar. However, the pressure dependence of k_{1a} remained unresolved.

Several experimental studies of reaction 1b have been reported in the literature.[4,7−10] All of these studies have involved shock tube measurements of time-dependent H-atom concentration profiles via atomic resonance absorption spectrometry and span the 1700−4000 K temperature range. Whereas Bhaskaran et al.[7] monitored H atoms in a shock tube study of C_2H_6/O_2 mixtures, Roth and co-workers[4,8] detected H atoms in shock-heated C_2H_6/Ar mixtures. At high temperatures, the ethane in the initial reaction mixture rapidly decomposes to yield CH_3, which generates H atoms via reaction 1b. The thermal reactions of CH_3 were also investigated by Lim and Michael[9] by detecting H atoms in reflected shock wave experiments using CH_3I/Kr

† Part of the special issue "James A. Miller Festschrift".

* Corresponding author: Venkatesh Vasudevan, Stanford University, Bldg 520, Room 520I, Stanford, CA, 94305-3032. Phone: 650-725-2042. Fax: 650-723-1748. E-mail: venkv@stanford.edu.

10.1021/jp0677187 CCC: $37.00
Published on Web 02/22/2007

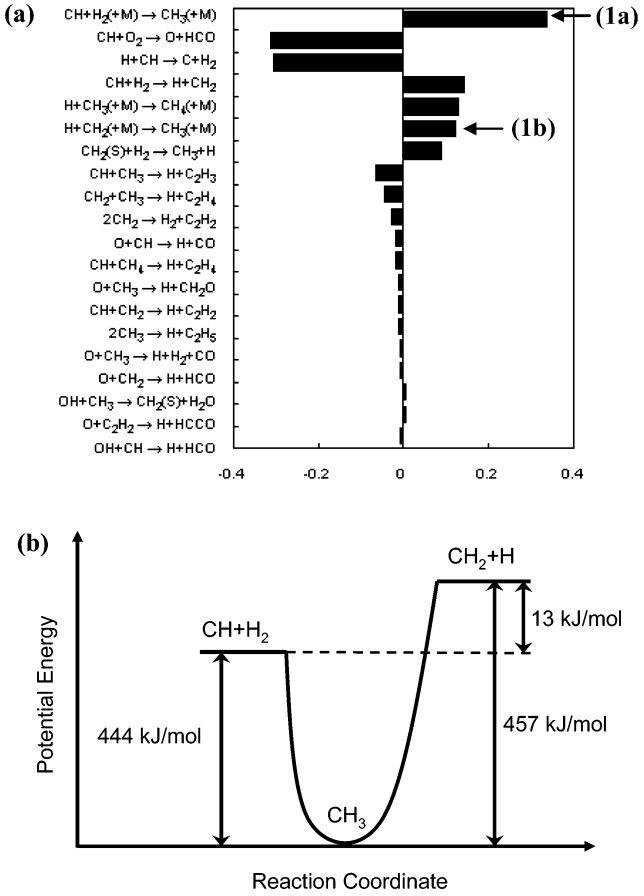

Figure 1. (a) Sensitivity to maximum CH concentration in shock tube oxidation of methane ($CH_4/O_2/Ar$ = 80 ppm/100 ppm/99.982%, ϕ = 1.6, P = 1.8 atm, T = 2800 K); adapted from ref 1, (b) Potential energy surface for methyl decomposition[10] (not to scale).

mixtures. In the 2150−2520 K temperature range, methyl decomposition to CH_2 + H was found to dominate H-atom formation; using detailed model simulations, Lim and Michael inferred rate coefficients for reaction 1b. Most recently, H atoms were monitored by Eng et al.[10] in incident and reflected shock wave experiments at pressures ranging from 0.1 to 4.8 bar and temperatures between 2000 and 4000 K, using highly dilute $CH_3N_2CH_3$/Ar and CH_3COCH_3/Ar mixtures to generate CH_3. Values for k_{1b} were obtained from the initial slope of the H-atom profiles. At temperatures below 2500 K, H-atom formation was dominated by secondary reactions, resulting in k_{1b} values much higher than those found in earlier work by Lim and Michael,[9] Roth and co-workers,[4,8] and Bhaskaran et al.[7]

Little direct experimental information is available on the branching ratio of methyl decomposition.[11] Markus et al.[4] measured both k_{1a} and k_{1b} in a single study, but there were uncertainties due to pressure effects in their measurements. Dean and Hanson[2] report Arrhenius expressions for both k_{1a} and k_{1b}; however, their CH measurements were not particularly sensitive to k_{1b}. Eng et al.[10] observed that the H-atom concentration approaches a stationary level, $[H]_\infty$, at long times. They obtained the branching ratio, $k_{1b}/(k_{1a} + k_{1b})$, by dividing this stationary H-atom concentration by the initial methyl-radical concentration. Unexpectedly high H-atom yields of up to 70% were observed at pressures of ∼1 bar; this could not be reconciled with the 25−45% high-pressure-limit branching ratio estimate of Fulle and Hippler[12] determined via studies of the reverse reaction.

Several theoretical studies of methyl decomposition have been reported (see ref 10 and references cited therein). The potential energy surface has been computed using ab initio methods and is presented in Figure 1b. Reaction 1a has a threshold that is 13 kJ/mol lower than reaction 1b and is therefore energetically favored. Both reactions proceed via "loose" transition states, i.e., they occur without any energy barrier. Whereas reaction 1b follows the least-motion pathway with C_{2v} geometry, reaction 1a follows a complicated non-least-motion pathway.[13] Two-dimensional, two-channel master equation calculations were recently reported by Eng et al.[10] These authors pointed out that the decomposition of methyl radicals must be in the falloff regime at ∼1 bar because both channels have been observed in experiments at this pressure (at the low-pressure limit, only reaction 1a, the energetically favored channel, should be accessible via collisions).[10] Therefore, there is the expectation of a possible pressure dependence in methyl decomposition at ∼1 bar, which is investigated in this study.

Clearly, direct high-temperature measurements of methyl decomposition are needed to provide accurate data on the overall rate and branching ratio, $k_{1b}/(k_{1a} + k_{1b})$. Also, uncertainty regarding the possible effect of pressure on methyl decomposition needs to be resolved. In this study, measurements were made behind reflected shock waves using narrow-line-width CH and OH laser absorption near 431.1 and 306.7 nm, respectively. Experiments were carried out at different pressures to study the effect of pressure on the two methyl decomposition pathways. Initial mixture compositions were chosen so that the measured CH and OH traces showed dominant sensitivity to reactions 1a and 1b, respectively. Rate coefficients were inferred by matching the experimental CH and OH concentration time histories with profiles modeled using detailed chemical kinetic mechanisms.

Experimental Setup

All experiments were carried out in the reflected shock region of a high-purity, stainless steel, helium-driven shock tube with an inner diameter of 14.13 cm. The shock tube facility is described in detail elsewhere.[14] Ethane (99%) and methyl iodide (>99.5%) were obtained from Specialty Chemical Products Inc. and Sigma Aldrich, respectively. Research-grade argon (99.9999%), helium (99.999%), and O_2 (99.999%) were supplied by Praxair Inc. Mixtures were prepared using partial pressures and were allowed to mix in a magnetically stirred mixing chamber to promote homogeneity and consistency. Because all of the mixtures used in this study were highly dilute, mixtures were prepared by successive dilution.[15]

The shock tube test section was pumped down to pressures on the order of 10^{-7} Torr before each experiment using a turbomolecular pump. Incident shock velocity measurements were made using five PZT pressure transducers and four programmable timer counters and linearly extrapolated to the endwall. Temperature and pressure in the reflected shock region were determined using one-dimensional shock calculations.

CH radicals were detected by continuous-wave, narrow-line-width ring dye laser absorption at 431.1311 nm. This wavelength corresponds to the overlapping $Q_{1d}(7)$ and $Q_{2c}(7)$ rotational lines of the CH A−X (0, 0) band.[16] Narrow-line-width radiation was generated by pumping a Coherent 699 ring dye laser, with stilbene 3 dye, with the multiline UV output from a Coherent Innova-200 Ar-ion laser. Single-mode operation of the laser was verified using a Spectra-Physics 470 scanning interferometer. The nominal laser wavelength was determined to within 0.01 cm^{-1} using a Burleigh WA-1000 wavemeter. The laser beam was split into two sections, a diagnostic beam and a reference beam. The two beams were balanced prior to each experimental run; this leads to effective common-mode rejection of laser intensity fluctuations and a minimum absorption detection limit of less than 0.1%.

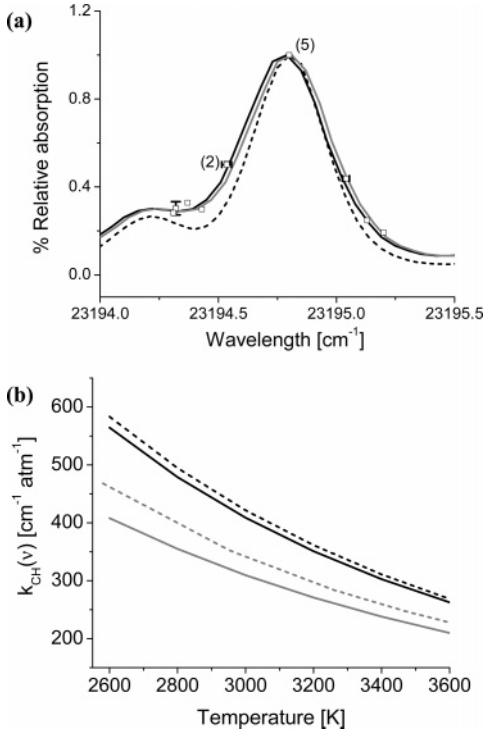

Figure 2. (a) LIFBASE simulation of the CH absorption feature near 23194.80 cm^{-1} (431.1311 nm) at 2800 K and 7.25 atm: dashed black line, $2\gamma_{CH-Ar} = 0.023$ cm^{-1} atm^{-1}; solid gray line, $2\gamma_{CH-Ar} = 0.034$ cm^{-1} atm^{-1}; solid black line, $2\gamma_{CH-Ar} = 0.034$ cm^{-1} atm^{-1} shifted by -0.015 cm^{-1}; open squares, experimental data from peak CH absorption during the pyrolysis of 20 ppm dilute ethane in argon. Numbers in parentheses correspond to the number of experiments performed at that wavelength. Vertical error bars represent ±10%; horizontal error bars represent ±0.02 cm^{-1}. (b) Comparison of current absorption coefficient calculation at 431.1311 nm (23194.80 cm^{-1}) with previous work: solid black line, this work, 1 atm; dashed black line, taken from Dean and Hanson,[16] 1 atm; solid gray line, this work, 4 atm; dashed gray line, taken from Dean and Hanson,[16] 4 atm.

OH radicals were monitored using a narrow-line-width ring dye laser tuned to the center of the $R_1(5)$ absorption line in the OH A−X (0, 0) band at 306.6871 nm. A 532-nm Coherent (Verdi) laser was used to pump Rhodamine-6G dye in a Spectra-Physics 380 ring dye laser cavity to generate 25−30 mW of visible light at 613.4 nm. The visible light beam was intracavity frequency-doubled in a temperature-tuned AD*A crystal to produce 1−2 mW of UV light near 306.7 nm. A detailed description of the OH diagnostic is available elsewhere.[14,17]

Quantitative OH and CH concentration profiles were generated from the raw traces of fractional transmission using Beer's law, $(I/I_o)_\nu = \exp(-k_\nu PXL)$, where I is the intensity of the transmitted laser beam; I_o is the intensity of the reference beam; k_ν is the absorption coefficient (atm^{-1}cm^{-1}) at frequency ν; P is the total pressure (atm); X is the mole fraction of the absorbing species, CH or OH; and L is the laser path length (14.13 cm). The absorption coefficient of the OH radical is well-established[17] and known to within ∼5%. The CH absorption coefficient was determined as described below.

CH Spectroscopic Model. A spectroscopic model, based on previous work by Dean and Hanson,[16] was used to establish the absorption coefficient of the CH radical. The CH absorption coefficient can be expressed as

$$k_{CH}(\nu) = \left(\frac{\pi e^2}{m_e c^2}\right)\sum\left[f_B\left(\frac{N_A}{RT}\right)f_{J''J}\Phi(\nu)\right] \qquad \text{(A)}$$

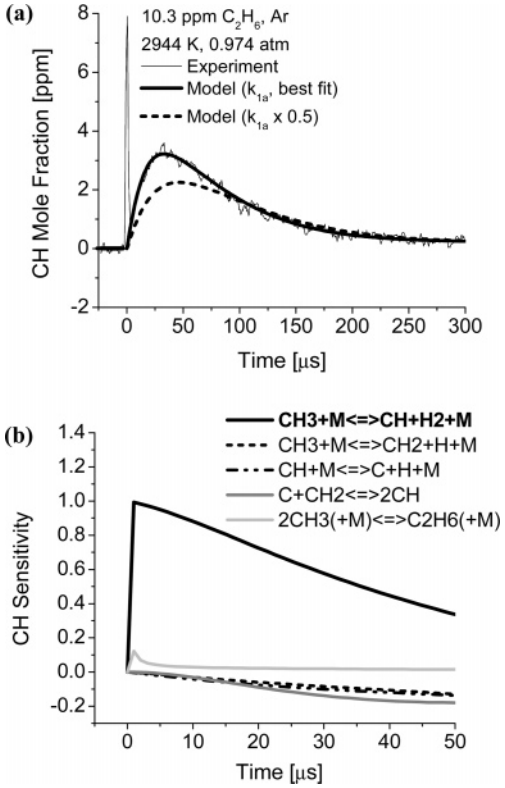

Figure 3. Example CH data, modeling, and sensitivity: (a) CH mole fraction time history; (b) CH-radical sensitivity at early times, $S = (dX_{CH}/dk_i)(k_i/X_{CH})$.

where $f_{J''J}$ is the rotational oscillator strength, f_B is the Boltzmann fraction of the population in the lower-energy state, N_A is Avogadro's number, R is the universal gas constant, and $\Phi(\nu)$ is the line shape factor (cm). The Boltzmann fraction can be calculated using the equation

$$f_B = (2J'' + 1)\exp\left[-\left(\frac{hc}{kT}\right)F(J'')\right]\exp\left[-\upsilon''\left(\frac{hc\omega_e}{kT}\right)\right]/Q \qquad \text{(B)}$$

where $F(J'')$ is the rotational energy of the lower-energy state, ω_e is the vibrational frequency, and Q is the total internal partition function. The total partition function is evaluated as a product of the rotational, vibrational, and electronic partition functions[16]

$$Q = Q_{rot}Q_{vib}Q_{elec} = \left(\frac{kT}{hcB''}\right)\left\{1 - \exp\left[-\left(\frac{hc\omega_e}{kT}\right)\right]\right\}^{-1}Q_{elec} \qquad \text{(C)}$$

where B'' is the rotational constant. The electronic partition function is $Q_{elec} = \sum\{g_e(n)\exp[-T_e(n)hc/kT]\}$, where $g_e(n)$ and $T_e(n)$ are the degeneracy and the electronic-term energy, respectively, of the nth electronic state. The electronic-term energy[18] of the ground doublet state is $T_e(X^2\Pi) = 0$ cm^{-1}, whereas for the lowest-lying excited quartet state, $T_e(a^4\Sigma^-) = 5844$ cm^{-1}. Higher electronic states (for example, $A^2\Delta$) do not contribute to the electronic partition function, even at temperatures as high as 5000 K. Population of the $a^4\Sigma^-$ quartet state would need to occur via collisions with argon, a spin-forbidden process that is not likely to occur in the time scale of our experiments (rate coefficients were typically inferred at $t < 50$ μs in the current work).[19] In the event that the system does thermalize rapidly, the contribution of the low-lying quartet state to Q_{elec} is ∼6% at 3000 K. This was included as an uncertainty

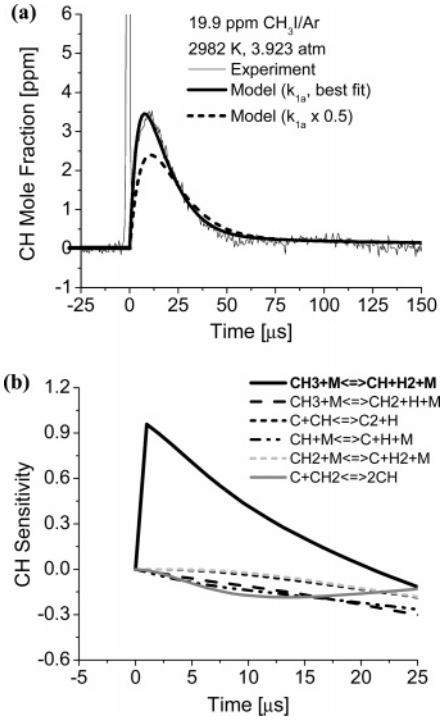

Figure 4. Example CH data, modeling, and sensitivity at high pressure: (a) CH mole fraction time history; (b) CH-radical sensitivity at early times, $S = (dX_{CH}/dk_i)(k_i/X_{CH})$.

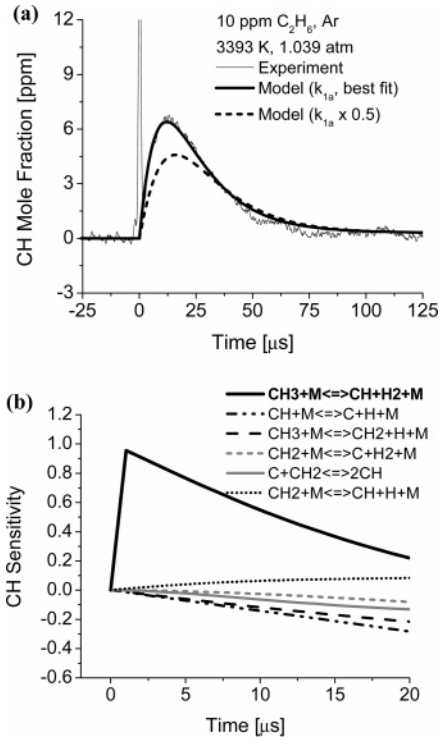

Figure 5. Example CH data, modeling, and sensitivity at high temperature: (a) CH mole fraction time history; (b) CH-radical sensitivity at early times, $S = (dX_{CH}/dk_i)(k_i/X_{CH})$.

in our absorption coefficient calculation where the electronic partition function was taken to be equal to the degeneracy of the ground state, $Q_{elec} \approx g_e(X^2\Pi) = 4$.[10,16]

Updated molecular and spectroscopic parameters were used to calculate the absorption coefficient as a function of temperature and pressure. Rotational and vibrational constants (ω_e and B'') and rotational-term energies [$F(J'')$] were taken from a recent study by Zachwieja et al.,[20] and rotational oscillator

TABLE 1: Rate Parameters for Reactions Sensitive during CH Formation and Removal

	rate coeff (cm^3 mol^{-1} s^{-1})			
reaction	*A*	*n*	*E* (kcal/mol)	ref
$CH_3 + M \rightarrow CH + H_2 + M$	see text			this work
$CH_3 + M \rightarrow CH_2 + H + M$	see text			this work
$CH + M \rightarrow C + H + M$	1.0×10^{14}	0	64.0	31[a]
$CH_2 + M \rightarrow C + H_2 + M$	1.15×10^{14}	0	55.8	31[a]
$H + CH \rightarrow C + H_2$	1.65×10^{14}	0	0.0	1
$C + CH \rightarrow C_2 + H$	2.0×10^{14}	0	0.0	31
$C + CH_2 \rightarrow 2CH$	1.0×10^{14}	0	0.0	31
$C + CH_3 \rightarrow H + C_2H_2$	5.0×10^{13}	0	0.0	1

[a] See text; rate coefficients were adjusted slightly (by up to ±25%) to match each measured CH decay.

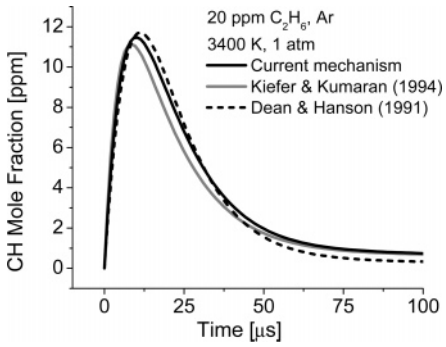

Figure 6. Comparison of CH time histories calculated using different hydrocarbon pyrolysis mechanisms. Initial reflected shock conditions: 3400 K, 1 atm; 20 ppm C_2H_6, balance Ar.

strength values were taken from Luque and Crosley.[21,22] The positions of the two lines that are of interest in this work, $Q_{1d}(7)$ and $Q_{2c}(7)$, were accurately measured by Brazier and Brown.[23] The line shape factor was evaluated using a Voigt profile for each CH transition.

Dean and Hanson,[16] in calculating the CH line shape, assumed the collision-broadening coefficient of CH in Ar, $2\gamma_{CH-Ar}$, to be equal to that of NH in Ar, $2\gamma_{NH-Ar}$ (0.023 cm^{-1} atm^{-1} at 2800 K), the latter having been measured accurately by Chang and Hanson.[24] This assumption is reasonable at ~1 atm, the pressure at which Dean et al.[25] performed all of their kinetic measurements, because the broadening is largely Doppler and the $2\gamma_{CH-Ar}$ value has only a small effect on the absorption coefficient at the line center. To the best of our knowledge, no direct measurements have been made of the pressure broadening of CH A−X transitions in argon. Takubo et al.[26] used a collision width of 0.07 cm^{-1} for CH A−X (0,0) for a propane/air flame, based on emission measurements by Rank et al.[27] and Harned and Ginsburg[28] in an oxyacetylene flame, while Luque et al.'s[29] examination of the CH A−X spectra of Peterson and Oh[30] suggests a collision width of <0.1 cm^{-1}.

In this study, the collision-broadening coefficient, $2\gamma_{CH-Ar}$, was inferred by measuring the absorption at discrete positions across the convolved CH line shape [overlapping $Q_{1d}(7)$ and $Q_{2c}(7)$ rotational lines] via repeated single-frequency experiments in the ethane pyrolysis system at 2800 K and 7.25 atm. The initial mixture was 20−21 ppm ethane in argon. The measured profile was simulated using LIFBASE[21] with the broadening coefficient as the only free parameter. Note that LIFBASE calculates the CH line shape using a Voigt profile, where the Voigt line is obtained by convolving the Gaussian (Doppler) and Lorentzian (collision) profiles. At 2800 K, a $2\gamma_{CH-Ar}$ value of 0.034 cm^{-1} atm^{-1} leads to a reasonable fit between the measured and simulated lineshapes (see Figure 2a); the measured $2\gamma_{CH-Ar}$ value is about a factor of 1.5 larger than

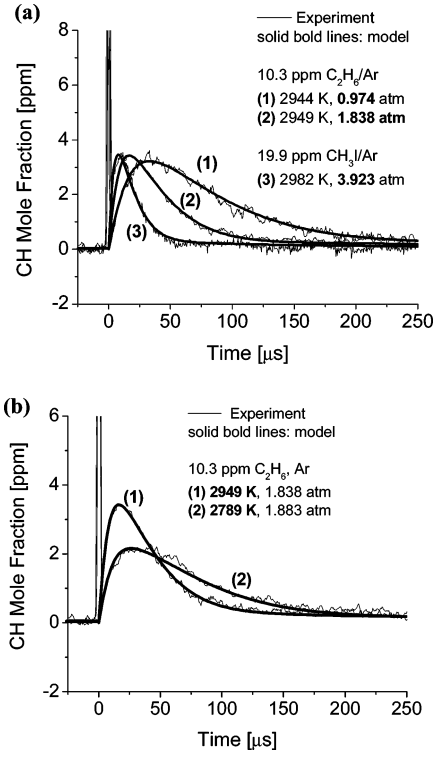

Figure 7. CH mole fraction time history: (a) pressure dependence, (b) temperature dependence.

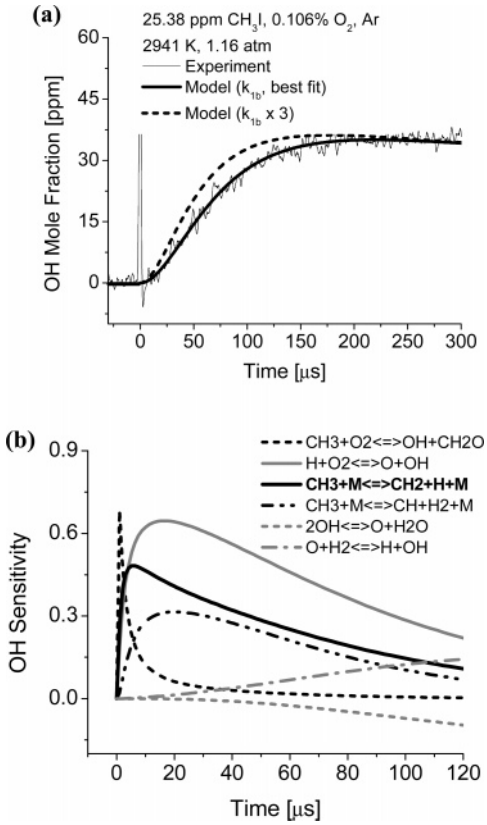

Figure 8. Example OH data, modeling, and sensitivity: (a) OH mole fraction time history; (b) OH-radical sensitivity at early times, $S = (dX_{OH}/dk_i)(k_i/X_{OH})$.

the value used by Dean and Hanson.[16] To reconcile the measurements, a small collision shift of between -0.01 and -0.02 cm^{-1} had to be included in the simulation. This collision shift is of the same order of magnitude and in the same direction as measured for other radical species such as OH in Ar [at 2800

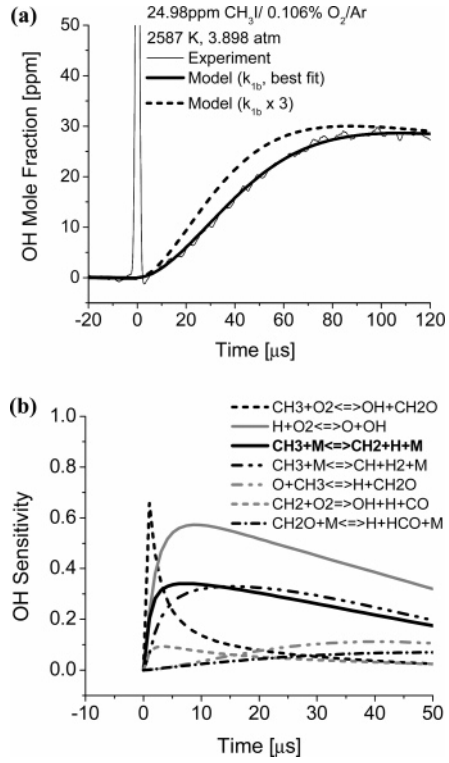

Figure 9. Example OH data, modeling, and sensitivity at high pressure: (a) OH mole fraction time history; (b) OH-radical sensitivity at early times, $S = (dX_{OH}/dk_i)(k_i/X_{OH})$.

K and 7.25 atm; recent measurements by Herbon et al.[15] suggest a collision shift of -0.04 cm^{-1} in the OH $Q_1(3)$ line]. It is pertinent to note that this shift borders on the ± 0.01 cm^{-1} resolution of the Burleigh WA-1000 wavemeter used in the current study. The uncertainty in the collision-broadening coefficient measurement is conservatively estimated at $\pm 20\%$. In the absorption coefficient calculation, the temperature dependence of the collision-broadening coefficient was assumed to be the same as that of NH, measured by Chang and Hanson.[24]

Figure 2b presents a comparison of the current absorption coefficient calculation with previous work by Dean and Hanson.[16] Agreement at 1 atm is good, as expected, because the higher $2\gamma_{CH-Ar}$ value has only a small effect on the absorption coefficient magnitude at this pressure, but at 4 atm, the present absorption coefficient calculation differs from that calculated by Dean and Hanson[16] by 10−15%.

At 2800 K and 4 atm, the overall uncertainty in the CH absorption coefficient is about $\pm 10\%$. This uncertainty is due to uncertainty in the following quantities: (a) CH oscillator strength ($\pm 3\%$), (b) collision-broadening coefficient ($\pm 20\%$), (c) electronic partition function ($\pm 5\%$), (d) temperature ($\pm 1\%$), and (e) pressure ($\pm 1\%$). A 3% change in the oscillator strength results in a ~3% change in $k_{CH}(\nu)$, whereas a 20% change in the broadening coefficient changes $k_{CH}(\nu)$ by ~8%. The absorption coefficient is not particularly sensitive to uncertainty in temperature and pressure: separate 1% changes in temperature and pressure result in changes of 2% and 0.4% in the absorption coefficient, respectively. Our uncertainty estimate for $k_{CH}(\nu)$ is conservative because the collision-broadening coefficient, the electronic partition function, and the temperature are likely known to better than $\pm 20\%$, $\pm 5\%$, and $\pm 1\%$, respectively. The combined uncertainty decreases at lower pressures, where most of the current experiments were carried out, because of the reduced influence of collision broadening.

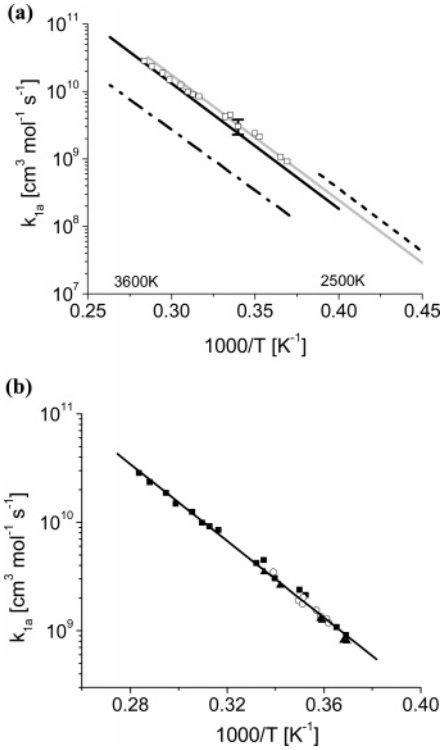

Figure 10. (a) Comparison of current measurements of k_{1a} with previous work: open squares, this work (±25% error bars), 0.7−1.1 bar; solid black line, Dean and Hanson,[2] 0.5−1.3 bar; dashed black line, Rohrig et al.,[3] 1.2 bar; dash-dotted line, Markus et al.,[4] 1.1−1.8 bar; solid gray line, Baulch et al.[11] (b) Pressure dependence of k_{1a}: solid squares, 0.7−1.1 atm data; open circles, 1.8−2.9 atm data; solid triangles, 3.6−4.2 atm data; solid black line, least-squares fit to data.

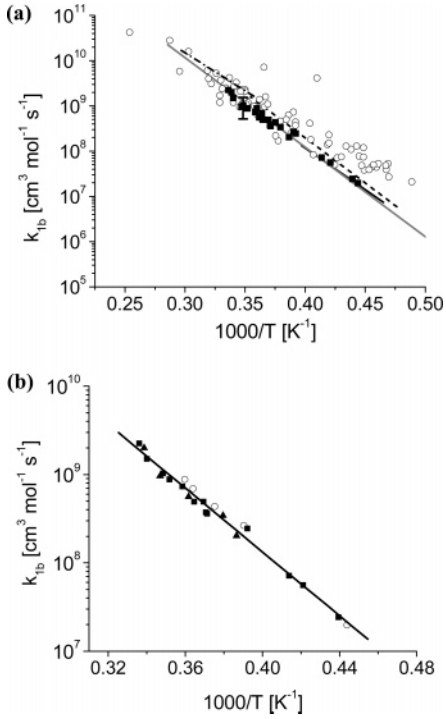

Figure 11. (a) Comparison of current measurements of k_{1b} with previous work: solid squares, this work (±50% error bars); open circles, Eng et al.;[10] dash-dotted line, Kiefer and Kumaran;[31] dashed line, Markus et al.;[4] solid black line, Lim and Michael;[9] solid gray line, Baulch et al.[11] (b) Pressure dependence of k_{1b}: solid squares, 1.09−1.41 atm data; open circles, 1.42−1.75 atm data; solid triangles, 2.99−3.89 atm data; solid black line, least-squares fit to data.

Kinetics Measurements

CH_3 + Ar → CH + H_2 + Ar. The rate coefficient of reaction 1a was measured by monitoring CH radicals generated upon shock-heating highly dilute mixtures of ethane, C_2H_6, or methyl iodide, CH_3I, in an argon bath. A detailed chemical kinetic mechanism was used to model the measured CH time histories and is described in greater detail in an ensuing section of this article. Initial mixture compositions were chosen such that the measured CH traces showed dominant sensitivity to reaction 1a at early times. The rate coefficient of this reaction was adjusted in the mechanism to yield the best fit between model and experiment. Figure 3a presents measured and modeled CH concentration profiles for an experiment conducted at 2944 K and 0.97 atm, and Figure 3b is a sensitivity analysis for this experiment. Sensitivity is defined as $(dX_{CH}/dk_i)(k_i/X_{CH})$, where X_{CH} is the local CH mole fraction and k_i is the rate coefficient of reaction i. Clearly, up to ∼50 μs, the most sensitive reaction is methyl decomposition to CH and H_2. Note that, in the sensitivity plot, the collision partner M is Ar.

Experiments were also carried out at higher reflected-shock pressures and temperatures. The CH profiles were primarily sensitive to reaction 1a at the earliest times. This is evident from Figure 4, which presents measured and modeled CH traces and the corresponding sensitivity plot for an experiment conducted at 3.9 atm and 2982 K. When compared to the lower-pressure experiment shown in Figure 3a, the time window over which reaction 1a has dominant sensitivity is shorter. Figure 5 presents results of a kinetic measurement performed at 3393 K and 1.039 atm; as expected, the sensitive time window is shorter at higher temperatures. Interference from unimolecular dissociation reactions, such as reactions 1b, 2, and 3, is somewhat higher at elevated temperatures and pressures.

$$CH + Ar \rightarrow C + H + Ar \quad (2)$$

$$CH_2 + Ar \rightarrow C + H_2 + Ar \quad (3)$$

In summary, for both the high-temperature and high-pressure experiments, k_{1a} could be accurately and reliably ascertained by fitting the measured profiles to a model at the earliest times ($t < 20$ μs).

Reaction Mechanism To Model CH Formation and Removal. In previous work, different reaction schemes have been used to model CH formation and removal in hydrocarbon pyrolysis systems. Dean and Hanson[2] used a two-channel scheme for CH_2 thermal decomposition with nearly equal rate coefficients for the two decomposition pathways, reactions 3 and 4, to model their CH and C-atom measurements.

$$CH_2 + Ar \rightarrow C + H_2 + Ar \quad (3)$$

$$CH_2 + Ar \rightarrow CH + H + Ar \quad (4)$$

However, Kiefer and Kumaran[31] were able to successfully model Dean's experiments using a very different reaction scheme consisting largely of rapid bimolecular reactions. In the Kiefer and Kumaran mechanism, the rate coefficient used for reaction 4 was about a factor of 10 smaller than that used by Dean and Hanson,[2] effectively eliminating the role of this reaction in the mechanism. That CH_2 decomposition favors reaction 3 was subsequently confirmed via measurements in the ketene pyrolysis system by Roth and co-workers.[32] In the current work, we have used a reaction scheme based on that of Kiefer and Kumaran, in which CH_2 decomposition results primarily in the

TABLE 2: Summary of Experimental Results, k_{1a}

T (K)	P (atm)	k_{1a} (cm^3 mol^{-1} s^{-1})
	10 ppm C_2H_6, balance Ar	
2837	1.042	2.14×10^9
2738	1.095	1.08×10^9
2984	1.005	4.49×10^9
3161	0.945	8.50×10^9
	10 ppm C_2H_6, balance Ar	
2858	0.976	2.39×10^9
2763	2.391	1.18×10^9
2845	2.637	2.03×10^9
2802	2.742	1.54×10^9
	10.3 ppm C_2H_6, balance Ar	
2789	1.883	1.36×10^9
2949	1.838	3.47×10^9
2861	1.907	1.90×10^9
2944	0.974	3.05×10^9
2717	3.829	8.12×10^8
2706	4.116	8.06×10^8
	19.99 CH_3I, balance Ar	
2848	1.835	1.77×10^9
2770	1.871	1.29×10^9
2982	3.923	3.48×10^9
2783	4.208	1.25×10^9
	10 ppm C_2H_6, balance Ar	
3393	1.039	1.87×10^{10}
3527	0.964	2.85×10^{10}
3230	1.024	9.91×10^9
3198	1.072	9.19×10^{10}
3273	1.013	1.25×10^{10}
3527	1.005	2.85×10^{10}
3472	1.040	2.35×10^{10}
3348	1.079	1.49×10^{10}
	10.09 ppm C_2H_6, balance Ar	
2709	1.087	9.11×10^8
3011	1.094	4.22×10^9
2925	3.580	2.63×10^9
2789	3.636	1.29×10^9

formation of C atoms and H_2. However, it is important to note that the reaction scheme used has little or no effect on our rate determination for reaction 1a. This is because, at the earliest times, CH is primarily sensitive only to reaction 1a; see Figures 3b, 4b, and 5b.

At later times, the CH profile is sensitive to several reactions; these include

$$CH_3 + Ar \rightarrow CH_2 + H + Ar \quad (1b)$$

$$CH + Ar \rightarrow C + H + Ar \quad (2)$$

$$CH_2 + Ar \rightarrow C + H_2 + Ar \quad (3)$$

$$H + CH \rightarrow C + H_2 \quad (5)$$

$$C + CH \rightarrow C_2 + H \quad (6)$$

$$C + CH_2 \rightarrow 2CH \quad (7)$$

$$C + CH_3 \rightarrow H + C_2H_2 \quad (8)$$

Even with the highly dilute reaction mixtures used in this study, it was not possible to unambiguously relate the decay in CH to a single dominant reaction. Hence, whereas the rate coefficients of the above reactions were constrained to match measured and modeled CH time histories over the temperature and pressure ranges of this study, these do not necessarily represent a unique set of reaction rate coefficients.

TABLE 3: Summary of Experimental Results, k_{1b}

T (K)	P (atm)	k_{1b} (cm^3 mol^{-1} s^{-1})
	25.38 ppm CH_3I, 0.106% O_2, balance Ar	
2780	1.425	8.82×10^8
2665	1.529	4.34×10^8
2562	1.600	2.66×10^8
2253	1.754	1.98×10^7
2747	1.488	6.93×10^8
2843	1.198	8.82×10^8
2698	1.242	3.73×10^8
2693	1.288	3.61×10^8
2550	1.285	2.45×10^8
2417	1.289	7.18×10^7
2375	1.370	5.61×10^7
2941	1.161	1.51×10^9
2276	1.409	2.43×10^7
	24.98 ppm CH_3I, 0.106% O_2, balance Ar	
2743	1.215	4.92×10^8
2765	3.698	5.61×10^8
2882	3.626	9.59×10^8
2587	3.898	2.03×10^8
2953	2.988	2.00×10^9
2635	2.991	3.42×10^8
	5.11 ppm C_2H_6, 0.103% O_2, balance Ar	
2707	1.191	4.93×10^8
2975	1.091	2.25×10^9
2871	1.119	1.03×10^9
2790	1.170	7.32×10^8

The mechanism and rate parameters used here are similar to those reported by Kiefer and Kumaran,[31] with some differences: (1) The rate coefficient for reaction 1b used by Kiefer and Kumaran was based on an RRKM calculation, whereas we used a value based on direct measurements that we carried out concurrently to determine k_{1b}. These experiments are described in an ensuing section of this article. Note that we did adjust our k_{1b} determination, within quoted uncertainty limits, to provide a best fit to each modeled and measured CH trace. (2) Minor adjustments were made to the rate coefficients of $CH_2 + Ar \rightarrow C + H_2 + Ar$ (~1.25 times the value of Kiefer and Kumaran) and $CH + Ar \rightarrow C + H + Ar$ (~1.25 times the value of Kiefer and Kumaran at $T < 3000$ K) to capture the measured CH decay. (3) Rate parameters for several reactions (for example, $C_2H_2 + Ar$, $C_2H_3 + Ar$, $C_2H_4 + Ar$, $CH_4 + Ar$, $H_2 + Ar$, $H + CH_4$, $H + CH_3$, $H + CH_2$, $H + CH$, $CH_3 + CH$, $CH_3 + CH_2$, $CH_3 + CH_3$, etc.) in the Kiefer and Kumaran mechanism were updated with more recent values from evaluations such as those of GRI-Mech 3.0[1]—all of these changes, however, had only a small effect on the modeled CH time histories. (4) The rate coefficient inferred for reaction 1a in this study was, on average, about 25% lower than that of Kiefer and Kumaran over the 2800−3600 K temperature range, with agreement being the poorest at low temperatures (~35% at 2800 K) and the best at high temperatures (~15% at 3600 K).

Table 1 summarizes the rate parameters employed in this study for the key reactions that control CH formation and removal in our experiments. That the current mechanism is largely consistent and in good overall agreement, at high temperatures, with earlier mechanisms developed by Dean and Hanson[2] and Kiefer and Kumaran[31] is evident from Figure 6, which presents modeled CH traces for an ethane pyrolysis experiment at 3400 K and 1 atm. The concentration chosen, 20 ppm ethane in argon, corresponds to that used by Dean and Hanson[2] in their ethane pyrolysis study.

Pressure and Temperature Dependence of CH Time History. Parts a and b of Figure 7 show the pressure and temperature dependences, respectively, of the CH time history.

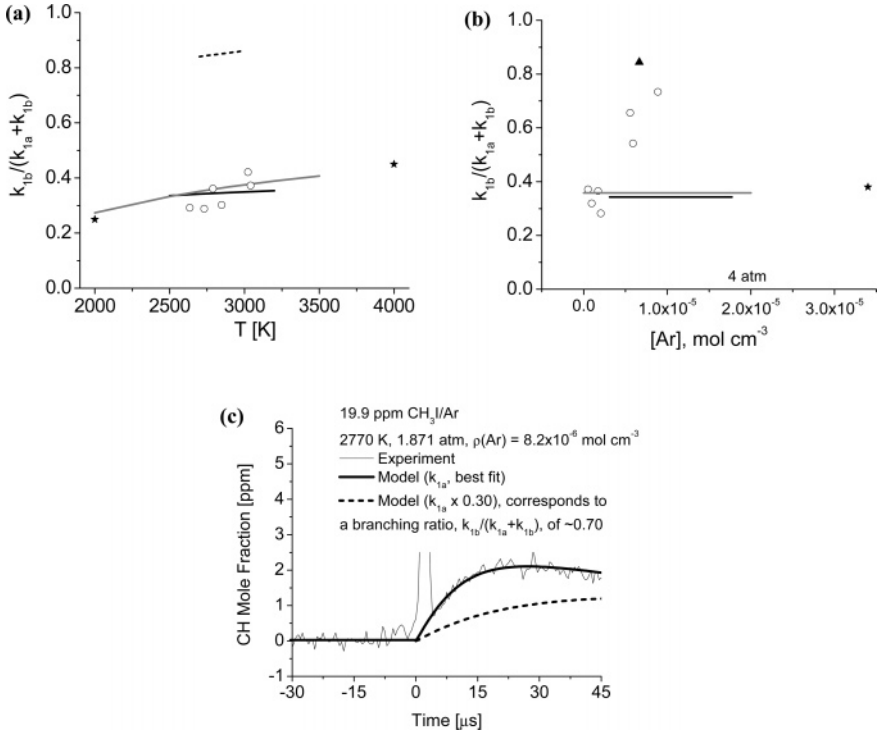

Figure 12. Branching ratio for the unimolecular decomposition of methyl radicals. (a) Temperature dependence: solid black line, this work; open circles, Eng et al.[10] [ρ(Ar) = 1.8×10^{-6} mol cm^{-3}]; solid stars, Fulle and Hippler[12] (high-pressure limit); dashed line, Markus et al.[4] (1.1−1.8 bar); solid gray line, Baulch et al.[11] (b) Pressure dependence at $T = 2750$ K: solid black line, this work; open circles, Eng et al.;[10] solid star, Fulle and Hippler[12] (high-pressure limit); solid triangle, Markus et al.;[4] solid gray line, Baulch et al.[11] (c) Effect of higher branching ratio on the modeled CH time history and comparison with experiment; a branching ratio of ~0.70 was reported by Eng et al.[10] at a comparable temperature and pressure (see Figure 12b).

At higher pressures and temperatures, the rise and decay in CH becomes faster. As temperature is increased, there is also a pronounced increase in the CH peak height; see Figure 7b. Clearly, our mechanism is able to capture the essential characteristics of the CH trace. Model performance, although satisfactory over the entire temperature and pressure range of the current study, was the poorest for experiments conducted at low temperatures and high pressures. In the worst case, decay times differed by 10−20% from experiment. However, this has little or no effect on the rate coefficients reported for reaction 1a, which were inferred using only the early-time CH rise.

CH_3 + Ar → CH_2 + H + Ar. The rate coefficient of reaction 1b was determined by shock-heating dilute mixtures of C_2H_6 or CH_3I and excess O_2 (0.1−0.5%) in argon. During the course of reaction, OH radicals were monitored using the well-characterized $R_1(5)$ line of the OH A−X (0, 0) band near 306.7 nm. H atoms generated via reaction 1b rapidly react with O_2, present in excess, forming OH. In the absence of secondary chemistry, the OH traces are primarily sensitive to reaction 1b and the reaction H + O_2 → OH + O. We used a similar measurement approach in a recent study to infer the overall rate coefficient and branching ratio for formaldehyde decomposition.[33] The kinetic strategy can be represented by the following simple reaction scheme

$$C_2H_6 \text{ or } CH_3I \rightarrow CH_3 + Ar \rightarrow CH_2 + H + Ar$$
$$+ O_2 \rightarrow \mathbf{OH} + O$$

Rate data were inferred by adjusting the rate coefficient of reaction 1b to match modeled OH profiles with experiment. A detailed chemical kinetic mechanism (GRI-Mech 3.0 with the Kiefer and Kumaran hydrocarbon pyrolysis model) was used to simulate the OH measurements. An example experimental profile is presented in Figure 8a, and Figure 8b shows the OH radical sensitivity analysis for this experiment. At early times, the OH profile shows reasonably strong sensitivity to reaction 1b. However, there is some secondary interference from reactions 1a and 9−11

$$CH_3 + Ar \rightarrow CH + H_2 + Ar \quad (1a)$$

$$H + O_2 \rightarrow OH + O \quad (9)$$

$$CH_3 + O_2 \rightarrow OH + CH_2O \quad (10)$$

$$O + H_2 \rightarrow H + OH \quad (11)$$

The rate coefficients of the three primary interfering reactions, reactions 1a, 9, and 10, are all relatively well-established. k_{1a} was carefully measured in this study to within approximately ±25% (the Arrhenius fit reported in this work was used in the current modeling). There have been several measurements of reaction 9, and recent studies[34] estimate an uncertainty of just 10% for k_9 over a broad temperature range. The rate expression recently recommended by Dryer and co-workers[35] for k_9 is in excellent agreement (within 10%) with the GRI-Mech 3.0 expression[1] used here. Reaction 10 was very recently studied in our laboratory by Herbon et al.[36] and is known to within approximately ±35%; the Arrhenius expressions recommended by Herbon et al. were used in the current modeling. Aside from reaction 11, minor secondary interference (not shown in Figure 8b) from the reactions 2OH → O + H_2O, CH + O_2 → O + HCO, CH_2 + O_2 → OH + H + CO, CH_2(s) + O_2 → OH + H + CO, CH_3 + O → H + CH_2O, and CH_2 + Ar → C + H_2 + Ar was observed. Conservative uncertainty estimates were used

TABLE 4: Thermochemical and Structural Parameters

parameter	value(s)
	CH_3
vibrational frequencies (cm^{-1})	3184, 3184, 3002, 1383, 1383, 580
moments of inertia (amu Å^2)	$I_A = I_B = 1.78$, $I_C = 3.60$
symmetry number	6
enthalpy of formation	$\Delta_f H_0$ (kJ mol^{-1}) = 149.7
electronic partition function	$Q_{elec} = 2$
	CH_2
vibrational frequencies (cm^{-1})	3123, 2954, 1056
moments of inertia (amu Å^2)	I_A= 0.231, ($I_B I_C$) = 2.19
symmetry number	2
enthalpy of formation	$\Delta_f H_0$ (kJ mol^{-1}) = 390.0
electronic partition function	$Q_{elec} = 3 + \exp(-3147\ cm^{-1} hc/k_b T) + \exp(-11497\ cm^{-1} hc/k_b T)$
	CH
vibrational frequencies (cm^{-1})	2861
moments of inertia (amu Å^2)	$I = 1.18$
symmetry number	1
enthalpy of formation	$\Delta_f H_0$ (kJ mol^{-1}) = 390.0
electronic partition function	$Q_{elec} = 2 + 2\exp(-17.9\ cm^{-1} hc/k_b T) + 4\exp(-4500\ cm^{-1} hc/k_b T)$
	H_2
vibrational frequencies (cm^{-1})	4395
moments of inertia (amu Å^2)	$I = 0.281$
symmetry number	2
enthalpy of formation	$\Delta_f H_0$ (kJ mol^{-1}) = 0
electronic partition function	$Q_{elec} = 1$
	H
symmetry number	1
enthalpy of formation	$\Delta_f H_0$ (kJ mol^{-1}) = 216.0
electronic partition function	$Q_{elec} = 2$

for the rate coefficients of these secondary reactions when setting error limits for our rate measurements. Note that, as temperature is reduced, sensitivity to reaction 1a diminishes whereas sensitivity to reaction 10 increases. This is because, at lower temperatures, methyl radicals are more likely to react with oxygen than decompose.

Experiments were also conducted to investigate the pressure dependence of reaction 1b. Results of a sample high-pressure measurement at 3.89 atm and 2587 K is shown in Figure 9. As in the low-pressure experiment described earlier (see Figure 8), the early-time OH concentration shows reasonable sensitivity to reaction 1b.

Results and Discussion

Our measurements of k_{1a} between 0.7 and 1.1 bar are presented in Figure 10a. The k_{1a} data are in good agreement with Dean and Hanson[2] and with a recent evaluation by Baulch et al.[11] The current high-temperature data are also consistent with the lower-temperature results of Rohrig et al.[3] The effect of pressure on the bimolecular rate constant is shown in Figure 10b. Within experimental uncertainty and scatter, a pressure dependence could not be discerned for k_{1a} in the 0.7−4 atm pressure range. A least-squares, two-parameter fit of the current measurements, valid over the 2706−3527 K temperature range, is given by the expression

$$k_{1a}\ (\mathrm{cm^3\ mol^{-1}\ s^{-1}}) = 3.09 \times 10^{15} \exp[-40700/T\ (\mathrm{K})]$$

The correlation coefficient of the above fit is −0.997, and the standard deviation is 0.038.

Figure 11a summarizes the current measurements of k_{1b} and previous work reported for this reaction rate coefficient. The k_{1b} data agree very well with the H-atom ARAS measurements of Eng et al.[10] at high temperatures and of Lim and Michael[9] at low temperatures. At temperatures lower than ∼2500 K, our measurements are in poor agreement with the data of Eng et al. These authors inferred k_{1b} using the initial slope of measured H-atom ARAS profiles. However, at low temperatures, reactions 12 and 13 contribute significantly to early-time H-atom formation, resulting in the observed high rate coefficient values.

$$CH_3 + CH_3 \rightarrow C_2H_5 + H \quad (12)$$

$$C_2H_5 \rightarrow C_2H_4 + H \quad (13)$$

Note that the current laser absorption data exhibit lower scatter than the H-atom ARAS measurements reported in the literature. Pressure dependence could not be discerned in the k_{1b} measurements (see Figure 11b) between 1.1 and 3.9 atm. A two-parameter, least-squares fit of the current data, valid over the 2253−2975 K temperature range, yields the rate expression

$$k_{1b}\ (\mathrm{cm^3\ mol^{-1}\ s^{-1}}) = 2.24 \times 10^{15} \exp[-41600/T\ (\mathrm{K})]$$

The correlation coefficient and standard deviation of the above fit are −0.992 and 0.071, respectively.

Even though no pressure dependence could be discerned for reactions 1a and 1b between 1 and 4 atm, this does not necessarily imply that the reactions are at the low-pressure limit because any pressure-dependent falloff might well be small and embedded within the scatter of the experimental data. The current k_{1a} and k_{1b} rate coefficient data are presented in Tables 2 and 3, respectively.

A detailed uncertainty analysis was carried out to set error limits for our measurements. The uncertainty factors taken into account were uncertainties in (a) wavemeter reading; (b) absorption coefficient of CH and OH; (c) initial mixture concentration; (d) reflected shock temperature, primarily due to uncertainty in shock velocity determination; (e) rate coefficients of secondary reactions; (f) fitting the modeled trace to the experimental profile; and (g) locating time zero. The effects of each of the above uncertainty categories on the rate coefficients of reactions 1a and 1b were ascertained and combined to yield overall uncertainty limits for both reactions. On the basis of this analysis, we conservatively estimate an uncertainty of ±25% in our k_{1a} measurement at 2944 K and 0.974 atm and an uncertainty of ±50% in our k_{1b} measurement at 2843 K and 1.198 atm. The uncertainty in k_{1a} is expected to be larger for our high-temperature (T > 3200K) and -pressure ($P \approx 4$ atm) experiments because of increased secondary interference from unimolecular decomposition reactions such as $CH_2 + Ar \rightarrow C + H_2 + Ar$ and $CH + Ar \rightarrow C + H + Ar$, while the uncertainty in k_{1b} is expected to be larger for our lower-temperature data because of increased interference from the $CH_3 + O_2$ reaction system and methyl radical recombination.

Parts a and b of Figure 12 present the branching ratio, $k_{1b}/(k_{1a} + k_{1b})$, as functions of temperature and pressure, respectively. The branching ratio for methyl decomposition is not well-established in the literature. Markus et al.[4] measured both k_{1a} and k_{1b} in a single study. However, their k_{1a} measurements are about a factor of 5 lower than the current data set (see Figure 10), resulting in a substantially higher branching-ratio value. In subsequent work, Markus et al.[6] reported an average k_{1a} value for pressures near 1 bar. When this expression for k_{1a} is used in conjunction with the Baulch et al.[11] recommendation for k_{1b} (based on several previous studies of k_{1b}, all of which are in good agreement[11]), the resulting branching ratio is in excellent agreement with that of the current work. The current branching-ratio measurements show no discernible dependence on pressure,

TABLE 5: Parameters for Multiwell Calculations at 2800 K

parameter	value
CH_3	
frequencies[a] (cm^{-1})	3184, 3184, 3002, 1383, 1383, 580
(*J*-rotor) adiabatic moments of inertia (amu Å^2)	1.78
(*K*-rotor) active external rotor (amu Å^2)	3.60
$CH_2\cdots H$ (transition state)	
critical energy at 0 K (kJ mol^{-1})	109.1
frequencies[a] (cm^{-1})	3123,2954,1056
(*J*-rotor) adiabatic moments of inertia (amu Å^2)	13.8
(*K*-rotor) active external rotor (amu Å^2)	3.60
moments of inertia active 2-D rotors (amu Å^2)	2.19
hindrance, η(2800 K)	90%
collision parameters: σ (Å^2), ϵ (K)	
CH_3	3.8, 144
Ar	3.47, 114
$<\Delta E>_d$(2800 K) (cm^{-1})	150
$CH\cdots H_2$ (transition state)	
critical energy at 0 K (kJ mol^{-1})	106.2
frequencies[a] (cm^{-1})	4395, 2861
(*J*-rotor) adiabatic moments of inertia (amu Å^2)	12.89
(*K*-rotor) active external rotor (amu Å^2)	3.60
moments of inertia active 2-D rotors (amu Å^2)	1.18 (CH rotor), 281 (H_2 rotor)
hindrance, η(2800 K)	98.7%
collision parameters: σ (A^2), ϵ (K)	
CH_3	3.8, 144
Ar	3.47, 114
$<\Delta E>_d$(2800 K) (cm^{-1})	150

in contrast to the results of Eng et al.,[10] who inferred branching ratios of up to 70% (see Figure 12b) from measured long-time H-atom plateaus. Our branching-ratio data are in very good agreement with the recent evaluation of Baulch et al.[11]

If the branching ratio were ~70%, as measured by Eng et al., CH peak levels would, according to detailed kinetic simulations, need to be about a factor of 2 lower than observed, with an early-time CH rise that is substantially slower than experiment. Note that, in the simulation, k_{1b} was kept fixed and k_{1a} was adjusted to yield a branching ratio of ~70%. The significant change in the temporal behavior of the CH profile at early times is illustrated in Figure 12c for an experiment at 2770 K and 1.871 atm. Such large differences cannot be explained by uncertainty in (a) experiment or (b) spectroscopic calibration of the CH diagnostic. To address the effect of pressure on the branching ratio, theoretical calculations using a master equation/RRKM analysis were carried out and are described in the next section of this article.

Master Equation/RRKM Analysis

Attempts were made to reproduce the experimental results with a master equation/RRKM analysis. This is in keeping with previous such attempts by Eng et al.[10] and Hippler et al.[37] The Multiwell suite[38,39] was used for the calculations, which were performed at 2800 K. The required parameters include thermochemical values for CH_3, CH_2, CH, H_2, and H. The values employed were the same as those used by Eng et al.[10] and are listed in Table 4. These values allow for the calculation of the equilibrium constants. The values obtained at 2800 K were $K_{-1b}(CH_2 + H = CH_3)$ (molecule cm^{-3}) = 2.97×10^{16} and $K_{-1a}(CH + H_2 = CH_3)$ (molecule cm^{-3}) = 1.26×10^{17}. The expressions in Fulle and Hippler[12] for the high-pressure-limit rate constants for the reactions as written above yield, for 2800 K, $k_{-1b\infty}$ (molecule cm^{-3} s^{-1}) = 4.5×10^{-10} and $k_{-1a\infty}$ (molecule cm^{-3} s^{-1}) = 2.8×10^{-10}. Thus, $k_{1b\infty}$ (s^{-1}) = 1.3×10^7 and $k_{1a\infty}$ (s^{-1}) = 3.5×10^7.

TABLE 6: Comparison of Calculated and Experimental Values at 2800 K and 1 atm

	$k_{1b}(CH_2 + H)$ (cm^3 mol^{-1} s^{-1})	$k_{1a}(CH + H_2)$ (cm^3 mol^{-1} s^{-1})	$k_{1b}/(k_{1a} + k_{1b})$
experiment	7.9×10^8	1.5×10^9	0.33
calculated	9.8×10^8	1.8×10^9	0.39

Values for calculation of the sums and densities of states of the transition states between CH_3 and the two channels that yield CH_2 + H and CH + H_2 were taken to reproduce the high-pressure rate parameters for the reverse processes from Fulle and Hippler[12] given above. The transitional modes were treated as hindered rotors in the hindered Gorin method as employed, for example, in Golden.[40] All parameters are reported in Table 5.

The centrifugal barriers were computed from the moments of inertia as explained in Golden.[40] Using a Morse potential, with the Morse β value computed using (for the CH_2 + H channel) the C−H stretching frequency in CH_3, the C−H bond distance, and the appropriate masses, the position of the centrifugal maximum was obtained by adding the rotational energy at the maximum, assumed to be *kT*, and finding the maximum. This led directly to a two-dimensional moment of inertia that could be used in the calculation of transition-state properties. For the transition state leading to CH + H_2, the potential is more complicated than a Morse function (see Mayneris et al.[41]), but the surface can be fit with a Morse potential at $CH-H_2$ distances greater than 1.33 Å. This was used as the starting point for computing the moment of inertia for that transition state. The probability for energy transfer was treated using the exponential down function.

When calculations were performed at 1 atm of Ar using the best inputs determined as above, the CH + H_2 channel did not appear. Because this is the channel with the more complex potential energy surface, the value for the two-dimensional moment of inertia in the transition state was modified until the correct branching ratio could be attained. This required a change from 11.0 to 12.89 amu Å.^{2} This change together with a value for ΔE_{down} of 150 cm^{-1} in the exponential down model could fit our data reasonably well. The results of a representative calculation are compared with the experimental values in Table 6. A pressure effect with a magnitude similar to that reported by Eng et al. could not be discerned in our calculation. Note that many parameter changes were tried (energy transfer was increased and decreased, Gorin hindrance was varied, the parameters were not required to fit the Fulle and Hippler reverse rate constant), but none yielded a significant pressure-dependent falloff.

Conclusions

Sensitive, narrow-line-width laser absorption diagnostics for CH and OH were used to perform measurements in the methyl decomposition system. Rate coefficients for the two methyl decomposition pathways, k_{1a} and k_{1b}, were measured with experimental conditions in the ranges 2253−3527 K and 0.7−4.2 atm. Within experimental uncertainty and scatter, no discernible dependence on pressure was observed in the rate coefficients of either pathway in the pressure and temperature ranges studied. The measurements are in very good agreement with the recent evaluation of Baulch et al.[11] Theoretical calculations carried out using a master equation/RRKM analysis fit the measurements reasonably well.

Acknowledgment. This work was supported by the Department of Energy, Office of Basic Energy Sciences, with Dr. Frank

Tully as contract monitor. The authors thank Dr. Jorge Luque (Lam Research), Dr. Jay Jeffries (Stanford University), Dr. Greg Smith (SRI International), and Dr. Sameer Naik (Purdue University) for useful discussions on CH spectroscopy.

References and Notes

(1) Smith, G. P.; Golden, D. M.; Frenklach, M.; Moriarty, N. W.; Eiteneer, B.; Goldenberg, M.; Bowman, C. T.; Hanson, R. K.; Song, S.; Gardiner, W. C., Jr.; Lissianski, V. V.; Qin, Z. *GRI-Mech 3.0*; Gas Research Institute: Chicago, IL, 2000; available at http://www.me.berkeley.edu/gri_mech/; website access date: August 2006.

(2) Dean, A. J.; Hanson, R. K. *Int. J. Chem. Kinet.* **1992**, *24*, 517.

(3) Rohrig, M.; Petersen, E. L.; Davidson, D. F.; Hanson, R. K.; Bowman, C. T. *Int. J. Chem. Kinet.* **1997**, *29*, 781.

(4) Markus, M. W.; Woiki, D.; Roth, P. *Proc. Combust. Inst.* **1992**, *24*, 581.

(5) Markus, M. W.; Roth, P. *Proc. Symp. Shock Waves* **1995**, *19*, 95.

(6) Markus, M. W.; Roth, P.; Just, Th. *Int. J. Chem. Kinet.* **1996**, *28*, 171.

(7) Bhaskaran, K. A.; Frank, P.; Just, Th. *Proc. Symp. Shock Waves* **1980**, *12*, 503.

(8) Roth, P.; Barner, U.; Loehr, R. *Ber. Bunsen-Ges. Phys. Chem.* **1979**, *83*, 929.

(9) Lim, K. P.; Michael, J. V. *Proc. Combust. Inst.* **1992**, *25*, 713.

(10) Eng, R. A.; Gebert, A.; Goos, E.; Hippler, H.; Kachiani, C. *Phys. Chem. Chem. Phys.* **2001**, *3*, 2258.

(11) Baulch, D. L.; Bowman, C. T.; Cobos, C. J.; Cox, R. A.; Just, Th.; Kerr, J. A.; Pilling, M. J.; Stocker, D.; Troe, J.; Tsang, W.; Walker, R. W.; Warnatz, J. *J. Phys. Chem. Ref. Data* **2005**, *34*, 757.

(12) Fulle, D.; Hippler, H. *J. Chem. Phys.* **1997**, *106*, 8691.

(13) Brooks, B. R.; Schaefer, H. F. *J. Chem. Phys.* **1977**, *76*, 5146.

(14) Vasudevan, V.; Davidson, D. F.; Hanson, R. K. *Int. J. Chem. Kinet.* **2005**, *37*, 98.

(15) Herbon, J. T. *Shock Tube Measurements of CH_3+O_2 Kinetics and the Heat of Formation of the OH Radical*; Mechanical Engineering Dept. Report TSD-153; Stanford University: Stanford, CA, 2004.

(16) Dean, A. J.; Hanson, R. K. *J. Quant. Spectrosc. Radiat. Transfer* **1991**, *95*, 183.

(17) Herbon, J. T.; Hanson, R. K.; Golden, D. M.; Bowman, C. T. *Proc. Combust. Inst.* **2002**, *29*, 1201.

(18) Huber, K. P.; Herzberg, G. *Molecular Spectra and Molecular Structure: IV. Constants of Diatomic Molecules*; Van Nostrand Reinhold Company: New York, 1979.

(19) Smith, G. P. SRI International, Menlo Park, CA. Teleconference on Nov 14, 2006.

(20) Zachwieja, M. *J. Mol. Spectrosc.* **1995**, *170*, 285.

(21) Luque, J.; Crosley, D. R. *LIFBASE: Database and Spectral Simulation Program*, version 1.5; SRI International Report MP 99-0099; SRI International, Menlo Park, CA, 1999.

(22) Luque, J.; Crosley, D. R. *J. Chem. Phys.* **1996**, *104*, 2146.

(23) Brazier, C. R.; Brown, J. M. *Can. J. Phys.* **1984**, *62*, 1563.

(24) Chang, A. Y.; Hanson, R. K. *J. Quant. Spectrosc. Radiat. Transfer* **1989**, *42*, 207.

(25) (a) Dean, A. J.; Hanson, R. K.; Bowman, C. T. *Proc. Combust. Inst.* **1990**, *23*, 955. (b) Dean, A. J.; Hanson, R. K.; Bowman, C. T. *J. Phys. Chem.* **1991**, *95*, 3180.

(26) Takubo, Y.; Yano, H.; Matsuoka, H.; Shimazu, M. *J. Quant. Spectrosc. Radiat. Transfer* **1983**, *30*, 207.

(27) Rank, D. H.; Saksena, D.; Wiggins, T. A. *J. Opt. Soc. Am.* **1958**, *48*, 521.

(28) Harned, B. W.; Ginsburg, N. *J. Opt. Soc. Am.* **1958**, *48*, 178.

(29) Luque, J.; Klein-Douwel, R. J. H.; Jeffries, J. B.; Smith, P.; Crosley, D. R. *Appl. Phys. B* **2002**, *75*, 779.

(30) Peterson, K. A.; Oh, D. B. *Opt. Lett.* **1999**, *24*, 667.

(31) Kiefer, J. H.; Kumaran, S. S. *J. Phys. Chem.* **1993**, *97*, 414.

(32) Markus, M. W.; Roth, P.; Tereza, A. M. *Proc. Combust. Inst.* **1994**, *25*, 705.

(33) Vasudevan, V.; Davidson, D. F.; Hanson, R. K.; Bowman, C. T.; Golden, D. M. *Proc. Combust. Inst.* **2007**, *31*, 175.

(34) Yu, C. L.; Frenklach, M.; Masten, D. A.; Hanson, R. K.; Bowman, C. T. *J. Phys. Chem.* **1994**, *98*, 4770.

(35) Li, J.; Zhao, Z.; Kazakov, A.; Dryer, F. L. *Int. J. Chem. Kinet.* **2004**, *36*, 566.

(36) Herbon, J. T.; Hanson, R. K.; Bowman, C. T.; Golden, D. M. *Proc. Combust. Inst.* **2005**, *30*, 955.

(37) Hippler, H.; Kachiani, C.; Olzmann, M. *Proceedings of the European Combustion Meeting*; Chauveau, C., Vovelle, C., Eds.; 2003.

(38) Barker, J. R. *Int. J. Chem. Kinet.* **2001**, *33*, 232.

(39) Barker, J. R.; Ortiz, N. F.; Preses, J. M.; Lohr, L. L.; Maranzana, A.; Stimac, P. J. *MultiWell-2.01 Software*; University of Michigan: Ann Arbor, MI, August 2006; available at http://aoss.engin.umich.edu/multiwell/.

(40) Golden, D. M. *Int. J. Chem. Kinet.* **2005**, *37*, 625.

(41) Mayneris, J.; Saracibar, A.; Goldfield, E. M.; Gonzalez, M.; Garcia, E.; Gray, S. K. *J. Phys. Chem. A* **2006**, *110*, 5542.